Received: 13 May 2021 | Revised: 2 November 2021 | Accepted: 14 November 2021

DOI: 10.1002/we.2698

RESEARCH ARTICLE

WILEY

OC6 Phase II: Integration and verification of a new soil–structure interaction model for offshore wind design

Roger Bergua[1] | Amy Robertson[1] | Jason Jonkman[1] | Andy Platt[1] | Ana Page[2] | Jacob Qvist[3] | Ervin Amet[4] | Zhisong Cai[5] | Huali Han[6] | Alec Beardsell[7] | Wei Shi[8] | Josean Galván[9] | Erin Bachynski-Polić[10] | Gill McKinnon[11] | Violette Harnois[12] | Paul Bonnet[13] | Loup Suja-Thauvin[14] | Anders Melchior Hansen[15] | Iñigo Mendikoa Alonso[16] | Ander Aristondo[16] | Tommaso Battistella[17] | Raúl Guanche[17] | Paul Schünemann[18] | Thanh-Dam Pham[19] | Pau Trubat[20] | Daniel Alarcón[20] | Florence Haudin[21] | Minh Quan Nguyen[21] | Akhilesh Goveas[22]

[1]National Wind Technology Center, National Renewable Energy Laboratory, Golden, Colorado, USA

[2]Advanced Modelling, Norwegian Geotechnical Institute, Oslo, Norway

[3]Department of Wind Energy, 4Subsea, Asker, Norway

[4]Wind Department, Bureau Veritas, Paris, France

[5]Integrated Simulation Department, China General Certification Center, Beijing, China

[6]Research Institute, CSIC Haizhuang Windpower Co., Ltd., Chongqing, China

[7]Offshore Technology Department, DNV, Bristol, UK

[8]State Key Laboratory of Coastal and Offshore Engineering, Dalian University of Technology, Dalian, China

[9]Department of Wind Energy, eureka!, Errigoiti, Spain

[10]Department of Marine Technology, Norwegian University of Science and Technology, Trondheim, Norway

[11]Department of Software Development, Orcina Ltd., Ulverston, UK

[12]Floating Offshore Group, PRINCIPIA, La Ciotat, France

[13]Solver R&D Department, Siemens Industry Software, Barcelona, Spain

[14]Department of Loads and Simulations, Simis AS, Malm, Norway

[15]Department of Wind Energy, Technical University of Denmark, Roskilde, Denmark

[16]Department of Offshore Renewable Energy, Tecnalia Research & Innovation, Donostia-San Sebastián, Spain

[17]IHCantabria - Instituto de Hidráulica Ambiental, Universidad de Cantabria, Santander, Spain

[18]Chair of Wind Energy Technology, University of Rostock, Rostock, Germany

[19]Department of Floating Offshore Wind Energy Generation Systems, University of Ulsan, Ulsan, South Korea

[20]Department of Civil and Environmental Engineering, Universitat Politècnica de Catalunya, Barcelona, Spain

[21]Research and Development Department, Vulcain Engineering, Neuilly-sur-Seine, France

[22]Department of Load Engineering, WyndTek, Delft, The Netherlands

Correspondence
Roger Bergua, National Renewable Energy Laboratory, 15013 Denver West Parkway, Golden, CO 80401, USA.
Email: roger.bergua@nrel.gov.

Funding information
US Department of Energy Office of Energy Efficiency and Renewable Energy Wind Energy Technologies Office, Grant/Award Number: DE-AC36-08GO28308

Abstract

This paper provides a summary of the work done within the OC6 Phase II project, which was focused on the implementation and verification of an advanced soil–structure interaction model for offshore wind system design and analysis. The soil–structure interaction model comes from the REDWIN project and uses an elastoplastic, macroelement model with kinematic hardening, which captures the stiffness and damping characteristics of offshore wind foundations more accurately than more traditional and simplified soil–structure interaction modeling approaches. Participants in the OC6 project integrated this macroelement capability to coupled aero-hydro-servo-elastic offshore wind turbine modeling tools and verified the implementation by comparing simulation results across the modeling tools for an example monopile design. The simulation results were also compared to more traditional soil–structure interaction modeling approaches like apparent fixity, coupled springs, and distributed springs models. The macroelement approach resulted in smaller overall loading in the system due to both shifts in the system frequencies and increased energy dissipation. No validation work was performed, but the macroelement approach has shown increased accuracy within the REDWIN project, resulting in decreased uncertainty in the design. For the monopile design investigated here, that implies a less conservative and thus more cost-effective offshore wind design.

KEYWORDS
hysteretic damping, macroelement, monopile, OC6, offshore wind, soil–structure interaction

1 | INTRODUCTION

As the wind industry moves to increasingly larger offshore wind turbines (OWTs) to lower cost, the associated support structures must similarly increase in size. One of the main challenges in designing fixed-bottom systems with large support structures is accurately representing the soil–structure interaction (SSI). The soil reaction is dependent on the foundation movement, and the foundation movement is dependent on the soil reaction. Thus, the SSI directly affects the dynamic response of the OWT system.

The foundation models traditionally used in integrated analysis of OWTs are simplistic and based on several assumptions. Most engineering tools model the foundation according to one of the following approaches: apparent fixity (AF), coupled springs (CS), or distributed springs (DS). The Norwegian Geotechnical Institute (NGI) has developed new macroelement models[1] for the SSI in OWTs that address some of the limitations in these previous models, allowing for a more accurate assessment of the dynamic response for OWTs. This development was done as part of the REDWIN (REDucing cost of offshore WINd by integrated structural and geotechnical design) project.[1]

The OC6 (Offshore Code Comparison Collaboration, Continued, with Correlation and unCertainty) Phase II project focuses on integrating the new REDWIN SSI modeling capability into coupled aero-hydro-servo-elastic modeling tools used to design offshore wind systems and verifying the new capability. OC6 is part of an ongoing effort under Wind Task 30 of the International Energy Agency (IEA) to verify and validate OWT modeling tools, which originated back in 2005 with the foundational OC3 project (Offshore Code Comparison Collaboration). In the current extension, OC6 is focused on examining specific physical phenomena that are not well represented in present modeling approaches and have a significant impact on their ability to accurately represent OWT loads and performance.

To verify the integration of the new REDWIN SSI capability, participants in OC6 Phase II modeled a monopile offshore wind system examined in the WAS-XL (Wave loads And Soil support for eXtra Large monopiles) project[2]; ran a series of simulations, including wind and wave loading; and compared the resulting system loads across different modeling tools. The resulting system loads were also compared to more traditional SSI modeling approaches to assess the level of difference that the macroelement modeling approach has on the global loads of the system. This paper summarizes the work of the OC6 Phase II project, including findings on the improvements the REDWIN model provides.

The organization of the remainder of the paper is as follows. Section 2 summarizes the different SSI models considered in the project, including the new REDWIN model. Section 3 provides a definition of the example model that was used to verify the implementation of the new SSI modeling capability. Section 4 provides a description of the active participants involved in OC6 Phase II and the modeling approach used. Section 5

then summarizes the load cases that were performed for the verification study. Finally, Sections 6 and 7 provide some example results from the project and the conclusions drawn.

The modeling information and simulation results from this project will be made available to the public by the end of 2021 through the US Department of Energy Data Archive and Portal, https://a2e.energy.gov/projects/oc6.

2 | SSI MODELS

In this section, an overview of the traditional methods for modeling SSI is given, and then, the new REDWIN modeling capability is introduced.

2.1 | Traditional methods

Aero-hydro-servo-elastic simulation tools are used during the design and certification of wind turbines.[3] During this process, thousands of load cases must be computed and analyzed. This requires these tools to be computationally efficient. In general, these simulation tools use relatively few DOFs, taking advantage of a combined modal and multibody dynamics formulation. Modeling the SSI in the time domain with a 3D finite element model would require thousands of additional DOFs, which would substantially increase the simulation time of the aeroelastic solver. Instead, traditional SSI approaches presently used within the offshore wind industry rely on simplified models, including AF, CS, or DS methods.

The AF method assumes that the substructure is fixed (cantilevered, without surrounding soil) at a depth below the original seabed, with a fixity depth and beam properties determined such that it matches the same lateral displacement and rotation at the seabed as the one resulting from the pile embedded in the true soil profile. The fixity depth and beam properties are dependent on the beam theory used (e.g., Euler–Bernoulli or Timoshenko). However, due to the nonlinear nature of the actual foundation, the response can only be identical under a particular set of conditions. The damping properties of the beams used in the AF method can also be modified to account for the energy dissipation provided by the SSI. Using the same structural damping as for the substructure may result in an underestimation of the fatigue lifetime.

The CS approach replaces the soil with one linear stiffness matrix located at the seabed that accounts for the six rigid-body degrees of freedom (DOFs) (or fewer) of the base of the monopile. This approach can reproduce the same results as the AF model and can be extended with a viscous damping matrix to account for the energy dissipated by the foundation.

The DS approach is the most sophisticated of the three approaches and can be considered the current practice in the wind industry to model soil–pile interaction. This approach was originally developed by the oil and gas industry, and it is recommended in many offshore design standards (e.g., Det Norske Veritas [DNV][4] and the American Petroleum Institute [API][5]). The method is based on the Winkler modeling approach. It employs uncoupled nonlinear springs represented by p–y curves to support the pile along the embedded depth. These springs relate the local lateral soil resistance (p) to the local lateral displacement of the pile (y). This relationship is commonly specified as semiempirical functions based on experimental tests. This approach characterizes four monopile DOFs (radial and bending directions). The vertical and torsional DOFs are usually fixed at the monopile base. It is also possible to add t–z curves in the vertical direction and torsional springs to define the six DOFs. Dashpot elements in parallel with the springs could be included to account for the foundation damping. This method was originally intended for static analysis, where the foundation response can be captured reasonably well with a nonlinear elastic curve, although the offshore wind industry takes advantage of the approach to perform dynamic analysis in situations where elastic models might not accurately capture the foundation response.

2.2 | REDWIN macroelement

The primary objective of the REDWIN project[1] was to develop soil-foundation models that better account for key geotechnical issues such as stiffness, damping, drainage, and degradation. Three soil-foundation models were developed considering the primary foundation types for OWTs, which can be coupled to time-domain simulation tools for offshore wind system design and analysis. The REDWIN approach is a CPU efficient way to couple the SSI capability into these tools, using as few DOFs as possible,[1] leading to a minimal increase in computational time while providing higher fidelity than traditional methods (AF, CS, or DS).

The goal of the OC6 Phase II project was to implement the REDWIN modeling approach in industry offshore wind modeling tools and verify the new capability by investigating an example offshore wind monopile design. REDWIN model 2 was used, which is a single macroelement approach that includes an elastoplastic model with kinematic hardening formulated within the multisurface plasticity framework.[6] It reduces the foundation and surrounding soil to a set of linear and nonlinear load–displacement relationships in the six DOFs of the interface point (the seabed), separating the foundation and the rest of the structure (see Figure 1). It can represent the nonlinear hysteretic load–displacement response observed in experimental tests and in the field, including the coupled response between horizontal loads and bending moments. The model has been demonstrated to give good agreement with results from finite element analyses of the soil and monopile, results from large-scale pile tests,

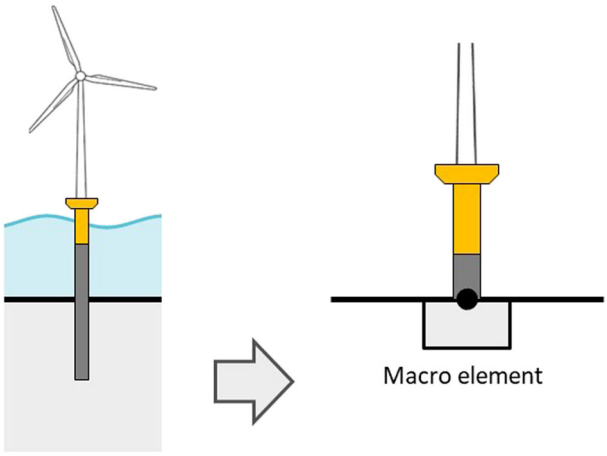

FIGURE 1 Illustration of the offshore wind turbine (left) and macroelement approach (right)[1]

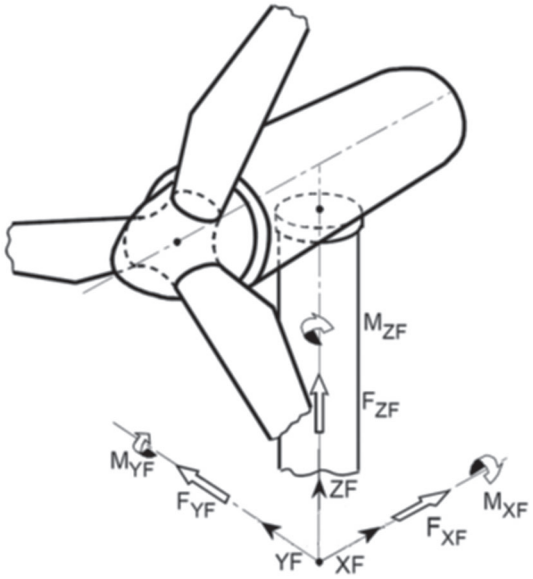

FIGURE 2 Global coordinate system

and results from full-scale field measurements of an OWT installed in the North Sea.[6–8] In addition, the macroelement model provides different stiffness after load reversal, as observed in pile tests.[9]

The REDWIN model provides an accurate representation of the foundation stiffness and hysteretic damping, which are important for accurately estimating fatigue. It is important to note that aerodynamic damping provides the highest contribution to the overall system damping in the fore–aft direction when the wind turbine is operating, but the aerodynamic damping importance decreases in idling and wind–wave misalignment situations, resulting in increased importance of soil damping.[10,11]

3 | EXAMPLE MODEL DEFINITION

To verify the integration of the REDWIN SSI approach into coupled OWT modeling tools, an example offshore wind system was modeled from the WAS-XL project.[2] WAS-XL is a project funded by the Norwegian Research Council focused on reducing the uncertainties in large-diameter monopile design by improving hydrodynamic models and soil stiffness and damping properties.

The global coordinate system used for defining the example OWT design and outputting results is given in Figure 2. The *x*-axis of the global Cartesian coordinate system points downwind with respect to the main wind and wave direction. The *z*-axis points upwards, and the *y*-axis forms a right-hand system.

To focus on the SSI, only the support structure was modeled in the OC6 Phase II project, and the rotor-nacelle assembly (RNA) is represented as a lumped mass and inertia. The properties are provided in Bergua et al.[12] and are based on the reference IEA-10.0-198-RWT wind turbine, a 10-MW, 198-m rotor diameter, direct-drive design.[13] The wind loading is approximated by supplying time histories of forces and moments at the yaw bearing. The tower[14] is based on the offshore DTU 10-MW wind turbine design and begins at an elevation of 40 m above the seabed. The water depth is 30 m, and the monopile substructure extends from the tower base to a penetration depth of 45 m. Figure 3 provides an overview of the design, and the exact dimensions for the tower and monopile, as well as the material properties, can be found in Bergua et al.[12]

The eigenfrequencies of the system for a clamped condition at the seabed (and no water) can be found in Table 1. The structural damping for the first bending mode including a rigid RNA is 0.5% critical damping. One percent critical damping is assumed for higher modes.

To model the foundation using REDWIN Model 2, two inputs are required: (1) the coefficients of the elastic stiffness matrix at the seabed and (2) two load–displacement curves at the seabed from a nonlinear pushover analysis. In addition, a few numerical parameters must be specified, which can be found in the OC6 Phase II project definition document.[12] The coefficients of the elastic stiffness matrix at the seabed are provided in Equation 1.

$$[K_{seabed\,6\times6}] = \begin{bmatrix} 6.336198E9 & 0 & 0 & 0 & -5.015421E10 & 0 \\ 0 & 6.336198E9 & 0 & 5.015421E10 & 0 & 0 \\ 0 & 0 & 1.119691E10 & 0 & 0 & 0 \\ 0 & 5.015421E10 & 0 & 8.111942E11 & 0 & 0 \\ -5.015421E10 & 0 & 0 & 0 & 8.111942E11 & 0 \\ 0 & 0 & 0 & 0 & 0 & 2.552673E11 \end{bmatrix}. \quad (1)$$

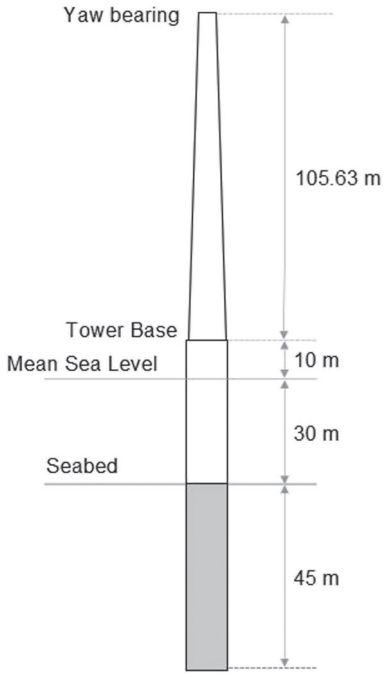

FIGURE 3 Schematic representation of the tower and monopile

TABLE 1 Approximate eigenfrequencies up to 2 Hz for the system clamped at seabed without water

Mode shape	Eigenfrequency (Hz)
First fore–aft bending mode	0.28
First side–side bending mode	0.28
Second fore–aft bending mode	1.44
Second side–side bending mode	1.33
First torsional mode	1.27

This stiffness matrix accounts for the six DOFs at the seabed, uses units of N, m, and rad and is expressed according to the coordinate system shown in Figure 2. The load–displacement curves used as input for the REDWIN macroelement model can be found in the project definition document.[12] These values were obtained from nonlinear pushover analyses performed with a quasi-static, three-dimensional finite element analysis. Models for the AF, CS, and DS methods can also be found in the project definition document.[12]

4 | PARTICIPANTS AND MODELING APPROACH

A total of 19 academic and industrial partners from 10 different countries actively participated in OC6 Phase II. Those actively involved were: the National Renewable Energy Laboratory (NREL, USA), 4Subsea (Norway), Bureau Veritas (BVEX, France), China General Certification Center (CGC, China), CSIC Haizhuang Windpower Co., Ltd. (CSSC, China), DNV GL (United Kingdom), Dalian University of Technology (DUT, China), eureka! (Spain), Norwegian University of Science and Technology (NTNU, Norway), Orcina (United Kingdom), PRINCIPIA (France), Technical University of Denmark (DTU, Denmark), Tecnalia (Spain), IH Cantabria (UC-IHC, Spain), University of Rostock (URO, Germany), University of Ulsan (UOU, Korea), Universitat Politècnica de Catalunya (UPC, Spain), Vulcain Engineering (France), and WyndTek (The Netherlands).

A list of the participants and the tools used in this study is provided in Table 2, which also shows the modeling approach employed.

As Table 2 shows, some participants decided to use more than one modeling approach and some used different codes. NREL used two different OpenFAST models (NREL 1 and NREL 2). NREL 1 models the tower by means of Euler–Bernoulli beams that account for the bending DOFs (ElastoDyn module) while NREL 2 models the tower by means of Timoshenko beams that account for axial, shear, bending, and torsion DOFs (SubDyn[15] module). A similar approach was adopted by eureka!. The EUREKA 1 model is equivalent to NREL 1, and EUREKA 2 is equivalent to NREL 2. The rest of the participants using OpenFAST adopted the same modeling approach as NREL 1.

There are three participants using the AF method: DUT 2, NREL 2, and WyndTek. The fixity depth and beam properties for this approach must be determined according to the beam theory used. NREL 2 and DUT 2 use Timoshenko beam elements and WyndTek uses Euler–Bernoulli

TABLE 2 Summary of participants, codes, and modeling approach used for the soil–structure interaction

		Soil–structure interaction approach			
Participant	**Code**	**AF**	**CS**	**DS**	**REDWIN**
4SUBSEA	OrcaFlex			X	
BVEX	Samcef WT			X	X
CGC	Bladed			X	
CSSC	OpenFAST				X
DNV GL	Bladed		X		X
DUT 1	OpenFAST				X
DUT 2	HAWC2	X		X	
DTU	HAWC2				X
EUREKA 1	OpenFAST		X		X
EUREKA 2	OpenFAST				X
NREL 1	OpenFAST				X
NREL 2	OpenFAST	X	X		X
NTNU	SIMA			X	X
ORCINA	OrcaFlex				X[a]
PRINCIPIA	DeepLines Wind				X
TECNALIA	OpenFAST		X		X
UC-IHC	OpenFAST				X
URO	OpenFAST				X
UOU	OpenFAST				X
UPC	FloaWDyn			X	X
VULCAIN	OpenFAST				X
WYNDTEK	Ashes	X		X	

Note: Orcina uses a built-in capability in OrcaFlex with some of the inputs from the REDWIN approach.

beams. Accordingly, NREL 2 and DUT 2 use the AF properties specified in the project definition document,[12] and WyndTek uses the properties corresponding to the improved AF method.

The participants modeling the SSI by means of the CS method use the stiffness matrix from Equation 1, and the participants using the DS approach use 61 discrete nonlinear springs defined every 0.75 m along the monopile. Each spring is defined by 22 pairs of p–y points. The numerical values of these p–y curves are available in the project definition document.[12]

The AF, CS, and DS approaches do not account for the SSI damping by default. To inform these methods, the equivalent SSI damping from the REDWIN approach was characterized at different loading levels by means of free-decay tests.[12] 4Subsea is the only participant using a traditional method (AF, CS, or DS) that includes damping for the SSI. 4Subsea includes viscous damping in the DS approach through dashpots with a constant damping coefficient in parallel with the springs. The damping coefficient is the same for all the dashpots and the same regardless of the loading condition. It is important to note that this viscous damping is proportional to the velocity while the hysteretic damping in the REDWIN approach is dependent on the displacement time history. The hysteretic damping of the REDWIN approach is also nonlinear; larger amplitudes translate into larger energy dissipated.[12]

Some participants decided to use some built-in capabilities in their codes to study the system. For example, Orcina uses a nonlinear hysteretic stiffness model available in OrcaFlex. In this case, only the diagonal positions of the stiffness matrix are populated. The nonlinear horizontal (K_{11},K_{22}) and rotational (K_{44},K_{55}) DOFs are defined according to the two load–displacement curves at the seabed from the nonlinear pushover analyses used as input for the REDWIN approach. The vertical (K_{33}) and torsional (K_{66}) DOFs are characterized based on the elastic stiffness matrix (see Equation 1). Although this approach results in a hysteretic behavior in the horizontal and rotational DOFs, these directions are uncoupled because the stiffness matrix used does not include cross-coupling coefficients. To avoid this, the location of the stiffness matrix is placed at a point along the monopile longitudinal axis below the seabed that induces a coupling between the horizontal and rotational directions.

5 | VERIFICATION METHODOLOGY

Similar to the OC3,[16] OC4,[17,18] and OC5[19–23] projects, a stepwise verification procedure was performed in the OC6 Phase II project. The model complexity is increased one step at a time to facilitate the identification of modeling discrepancies introduced by different theories and/or model implementations in the various codes. Table 3 provides a summary of the simulations that are presented in Section 6, including static simulations (1.X), eigenanalyses (2.X), wind-only simulations (3.X), wave-only simulations (4.X), and combined wind/wave simulations (5.X). The complete list of load cases studied can be found in the project definition document.[12]

It is important to note that the responses from load cases that involve wind (i.e., Load Case 3.1 and Load Case 5.1) are used for verification purposes but cannot be considered representative of a real wind turbine in operating conditions due to the lack of aerodynamic damping in the models used in this code-to-code verification.

TABLE 3 Offshore Code Comparison Collaboration, Continued, with Correlation and unCertainty (OC6) Phase II load case simulations (summary)

Analysis type	Load case	Enabled degrees of freedom	Wind conditions	Marine conditions	Comparison type
Static	1.2	Tower, substructure, foundation	None	None	Static response
Eigenanalysis	2.3	Tower, substructure, foundation	None	Still water	Frequencies, damping, and mode shapes
Wind only	3.1	Tower, substructure, foundation	Prescribed load time series at yaw bearing $V_{hub} = 9.06$ m/s	None	Time series ($t = 3600$ s)
Wave only	4.2	Tower, substructure, foundation	None	Irregular waves: Pierson–Moskowitz wave spectrum $H_s = 1.25$ m, $T_p = 5.5$ s	Time series ($t = 3600$ s)
Wind + waves	5.1	Tower, substructure, foundation	Prescribed load time series at yaw bearing $V_{hub} = 9.06$ m/s	Irregular waves: Pierson–Moskowitz wave spectrum $H_s = 1.25$ m, $T_p = 5.5$ s	Time series ($t = 3600$ s)

Note: H_s: significant wave height; T_p: peak-spectral wave period; V_{hub}: average hub height wind speed; t: time.

6 | SELECTED RESULTS

In this section, a comprehensive overview of the studied load cases shown in Table 3 is presented and explained.

6.1 | Static simulations results: Load Case 1.2

Load Case 1.2 focuses on ensuring that the structural model was implemented correctly by examining the static loads and deflections of the system with gravity acceleration as the only external loading.

Figure 4 shows the tower-top (yaw bearing) displacement along the *x*-axis (fore–aft direction) under gravity-only conditions. This displacement is the result of the overhanging weight of the RNA, and it is affected by the SSI stiffness. The dashed black line shows the average displacement from all participants and it can be used as a reference to compare the different solutions.

As Figure 4 shows, the linear SSI approaches (AF and CS) result in smaller tower-top displacements. These linear approaches were characterized based on the unloaded state (see Equation 1) and behave slightly stiffer than the nonlinear SSI approaches. Interestingly, WyndTek AF using the improved AF method (Euler–Bernoulli beams) and NREL 2 AF using the AF method (Timoshenko beams) produce the same displacement. The tower-top displacements for the DS approach are slightly bigger due to the nonlinearity of the *p*–*y* curves. Finally, the REDWIN shows slightly larger displacements than the DS approach because it accounts for the nonlinear stiffness and plasticity. Not all the simulation tools are able to perform a static analysis or gradually apply the gravity acceleration in a quasi-static fashion. Accordingly, some participants perform a transient analysis where the gravity acceleration is suddenly applied over the system at the beginning of the simulation. This results in an initial transient loading that can induce a small level of plasticity. Therefore, REDWIN solutions using an initial static computation or a gradual loading result in slightly smaller displacements closer to the DS approach.

6.2 | Eigenanalysis Results: Load Case 2.3

Load Case 2.3 furthers the examination of the structural model by assessing the system eigenfrequencies, damping values, and mode shapes. Figures 5 and 6 show the system eigenfrequencies for the first and second bending modes in the fore–aft direction. These outputs are from Load Case 2.3, which includes foundation flexibility and still water conditions. For reference, the plots include a gray dashed line with the average result when the foundation is considered rigid (i.e., clamp at seabed), and there are no marine conditions (i.e., no water). These average results were obtained from the results provided by the participants in Load Case 2.1 (see the project definition document[12] for reference) and are aligned with the numerical values from Table 1. The black dashed line denotes the average solution when accounting for the foundation flexibility and marine conditions (i.e., still water).

As Figure 5 shows, the first bending mode drops around 10% in frequency due to the flexible foundation. The water does not have a significant impact for the first bending mode in this system. For the second bending mode (Figure 6), the drop in frequency is around 20% on average.

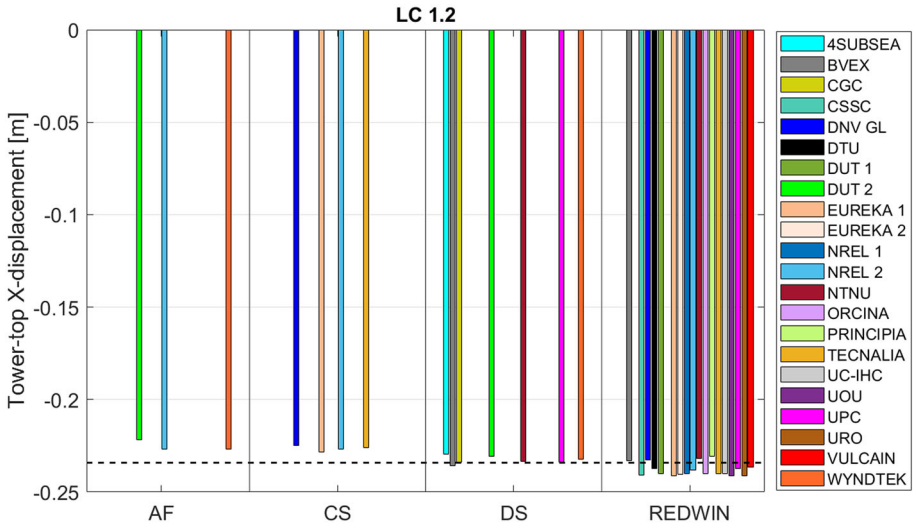

FIGURE 4 Tower-top X-displacement for gravity-only conditions in load case (LC) 1.2

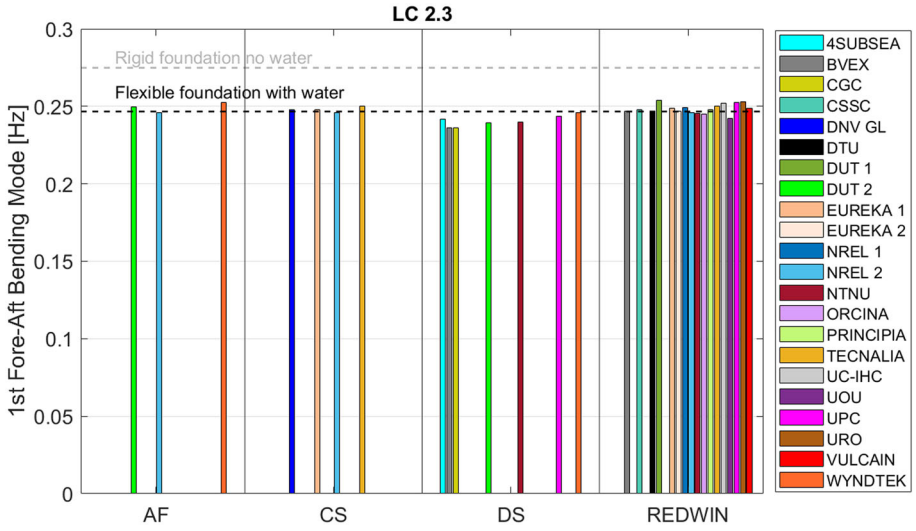

FIGURE 5 First fore–aft bending mode eigenfrequency depending on the soil–structure interaction approach in load case (LC) 2.3

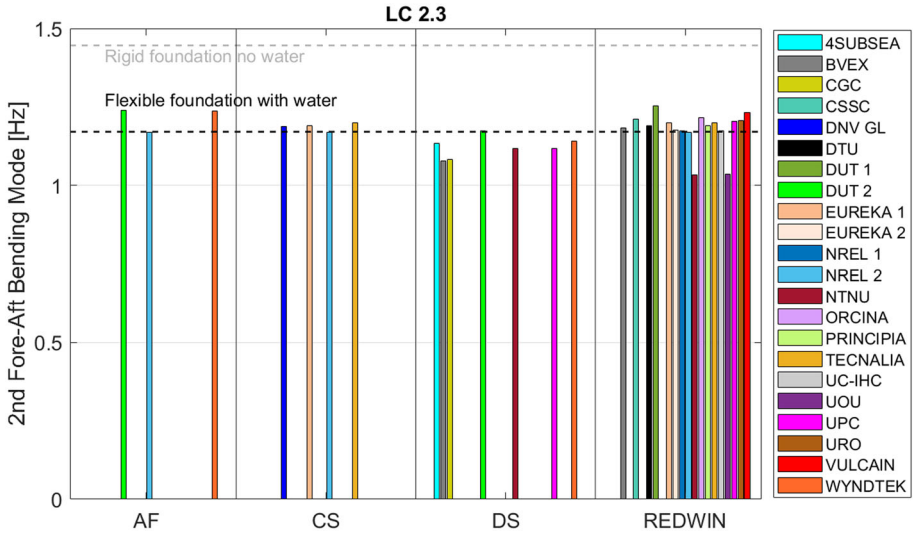

FIGURE 6 Second fore–aft bending mode eigenfrequency depending on the soil–structure interaction approach in load case (LC) 2.3

The main reason for this drop in frequency is also the foundation flexibility, but the added mass from the still water is also noticeable. In the studied system and for all load cases, the monopile does not have water inside. Having the monopile filled with water would decrease these eigenfrequencies further.

There is a good agreement between participants for the first bending mode in the fore–aft direction. The linear approaches (AF and CS) behave slightly stiffer than the DS approach as expected and observed during the static analysis (i.e., Load Case 1.2). A similar trend can be observed in Figure 6 for the second bending mode. It is also interesting to note that in this second bending mode, the agreement between participants is not as good as for the first bending mode. One of the reasons for the dispersion in the eigenfrequencies between participants using the same SSI approach is the method used to extract the eigenproperties around the static equilibrium. Some simulation tools used by the participants include a linearization capability, while other participants without this functionality tried to obtain these properties from time-domain simulations (e.g., by means of a free-decay test or a broadband wind or wave excitation). For example, Figure 6 shows some significant differences between some of the participants using the REDWIN approach. However, when postprocessing the time-domain results of Load Case 5.X in the frequency domain, these differences were not observed (see, e.g., Figures 17 and 19). Extracting the eigenproperties of a model using the REDWIN approach can be challenging due to the nonlinear nature of the system.

Figure 7 shows the associated eigenvectors of the first and second bending modes in the fore–aft direction. The eigenvectors are normalized by their maximum amplitude to allow the comparison between participants.

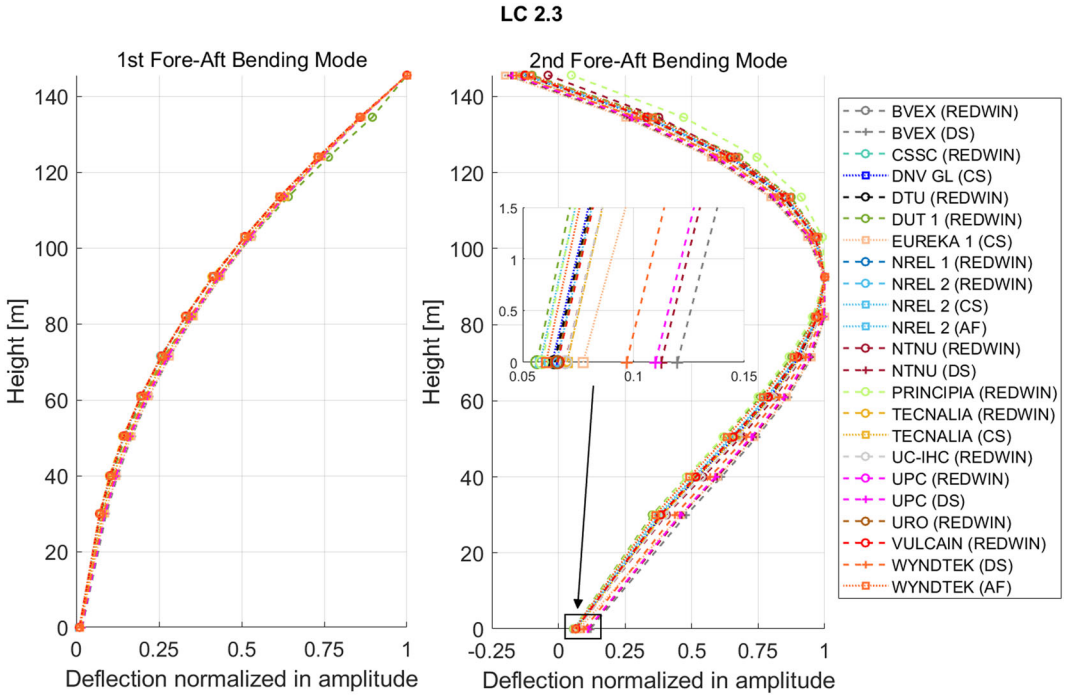

FIGURE 7 Eigenvectors of the first and second fore–aft bending modes in load case (LC) 2.3

As expected, the largest amplitude for the first bending mode is located at the tower top. As seen in Figure 7, the agreement between the participants is very good regardless of the SSI approach used. For the second bending mode, the maximum amplitude occurs at about two thirds of the support structure height. In this case, all the participants using the DS approach have slightly more deflections at the seabed ($h = 0$ m).

6.3 | Wind-only simulations results: Load Case 3.1

After analyzing the static cases and the eigenproperties of the system, the response under wind-only conditions was studied. The environmental conditions in Load Cases 3–5 are representative of a 30-m water depth site at the Norwegian Continental Shelf.[11]

As noted in Section 3, the computational models account for the support structure and a lumped mass and inertia for the RNA. The wind loading in the six DOFs for Load Cases 3.1 and 5.1 (see Table 3) was computed beforehand by NREL and was applied as external force and moment time histories by participants at the yaw bearing (see the project definition document[12] for further details).

Load Case 3.1 is a wind-only load case and considers a mean wind speed at hub height (V_{hub}) of 9.06 m/s. This wind speed is below the rated wind speed of 10.75 m/s[13] for the IEA-10.0-198-RWT. Under these conditions, the wind turbine is rotating at about 7.75 rpm. The aeroelastic model used to compute the externally applied loads did not include any rotor imbalance (e.g., no mass nor aerodynamic imbalance). Accordingly, the only excitations present in the computed loads correspond to the blade passing frequency (3P for a three-bladed wind turbine) and the corresponding harmonics (e.g., 6P and 9P), where P is the rotor speed.

The power spectral density (PSD) of the tower-top acceleration along the *x*-axis (fore–aft direction) is shown in Figure 8. The main excitations (i.e., 3P, 6P, and 9P) and the eigenfrequencies (i.e., first and second fore–aft bending modes) are also included with vertical dashed lines in the figure. The eigenfrequencies are marked according to the average solution from all participants in Load Case 2.3 (Figures 5 and 6). It is important to note that Load Case 2.3 includes the marine conditions but Load Case 3.1 does not. However, the same vertical lines were used for the eigenfrequencies for an easier comparison against the results from Load Case 5.1.

Different line styles are used in the spectrum to compare the different approaches. The solutions using a linear SSI approach (AF or CS) are denoted with a dotted line, the ones using the DS approach are denoted with a dashed line, and the ones using the REDWIN approach are denoted with a solid line. In the legend, participants using different modeling approaches appear with the line style associated with its highest model fidelity used (REDWIN > DS > AF|CS).

For this loading condition, the 9P excitation is virtually at the same frequency as the second fore–aft bending mode. This resonance can lead to increased levels of structural activity at this frequency.

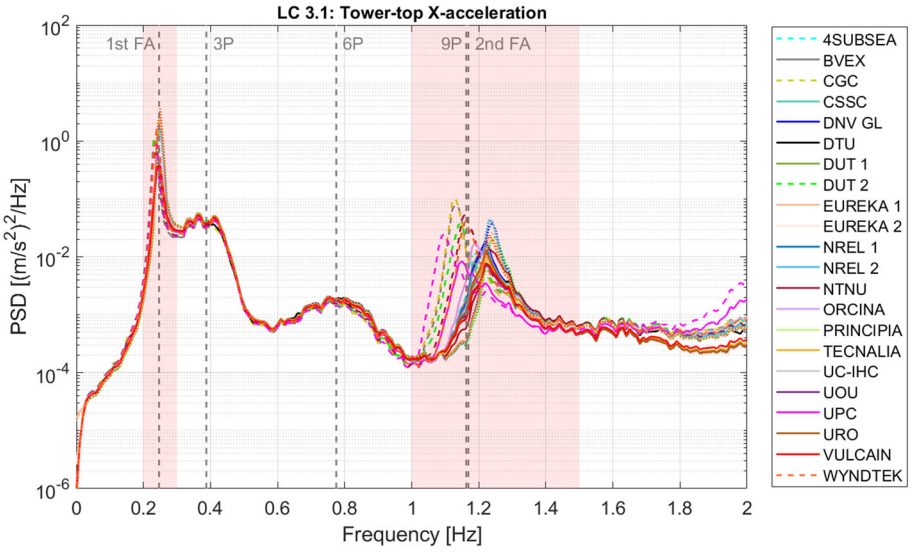

FIGURE 8 Power spectral density (PSD) of the tower-top X-acceleration in load case (LC) 3.1

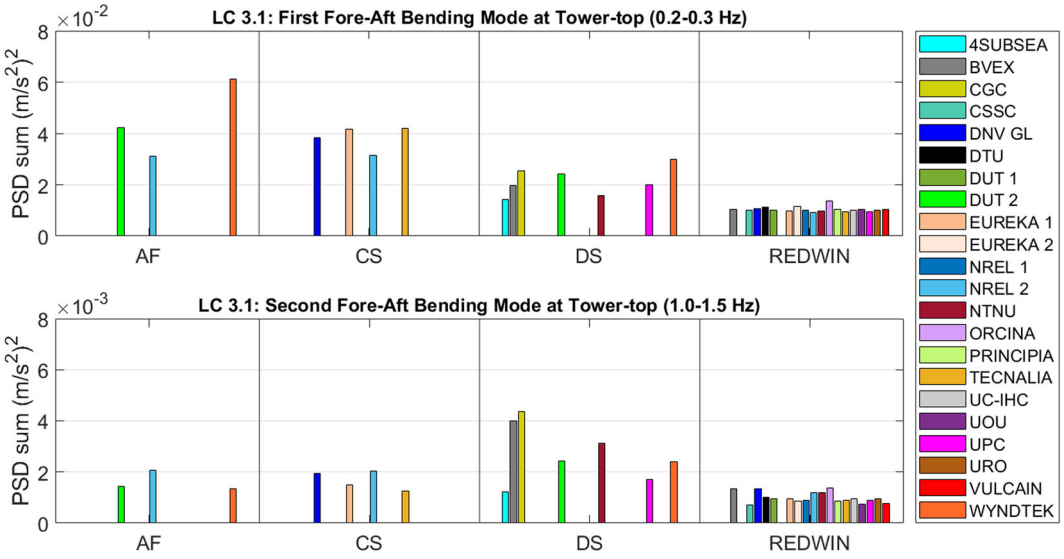

FIGURE 9 Power spectral density (PSD) sums of the tower-top X-acceleration in load case (LC) 3.1

The agreement between participants for the first fore–aft bending mode eigenfrequency is very good with only some differences in terms of amplitude. For the second fore–aft bending mode, some differences in terms of frequency can be observed. The linear SSI approaches (AF and CS) show the stiffest behavior and the DS approach the softest. For this second bending mode, the DS approach also has the largest amplitude.

To more systematically compare the response between participants and modeling approaches, the PSD sum (Equation 2) is computed based on the one-sided, unsmoothed, discrete power density functions.

$$S_{sum} = \sum_{i=j}^{k} S_{resp}(f_i)\Delta f, \tag{2}$$

where $S_{resp}(f_i)$ is the discrete PSD amplitude at frequency f_i, Δf is the frequency resolution, and j and k are the indices of the first and last frequency of interest. This PSD sum is equivalent to the integral of the PSD for a given frequency range. For reference, the square root of this PSD sum is equivalent to the root mean square (RMS) for the frequency range of interest.

Two PSD sum magnitudes are computed to analyze the results in more detail: one for the frequency range between 0.2 and 0.3 Hz and the other between 1.0 and 1.5 Hz. These two frequency ranges are marked with two red rectangles in Figure 8 and can be considered indicative of the first and second fore–aft bending mode responses. Figure 9 shows the PSD sums for the different participants according to the SSI approach used. The *y*-axis scale for the first frequency range (0.2–0.3 Hz) is one order of magnitude higher than for the second frequency range (1.0–1.5 Hz) to highlight the relative importance of the first bending mode response compared to the second bending mode.

For the first fore–aft bending mode, the largest response corresponds to the linear SSI approaches. These linear approaches result in a slightly stiffer system, which places the first structural mode closer to the 3P excitation. The DS approach has a smaller response than the linear SSI approaches but a larger response than the REDWIN due to the lack of damping. For the second fore–aft bending mode, the smallest response also corresponds to the REDWIN approach. 4Subsea also uses the DS approach, but it includes SSI damping. By including this damping, the response is the smallest of the DS solutions for the first and second fore–aft bending modes and is at a level that is quite similar to the REDWIN approach. The results across the REDWIN solutions are very similar, showing comparable trends for the remaining load cases.

Figure 10 shows the monopile fore–aft bending moment at the seabed and Figure 11 the associated PSD sums. The main difference in this case is the behavior at 0 Hz. This amplitude is indicative of the signal average; the mean fore–aft bending moment at the seabed in this case. This mean value is mainly driven by the aerodynamic thrust force acting over the system. For the acceleration, the mean value will always be zero.

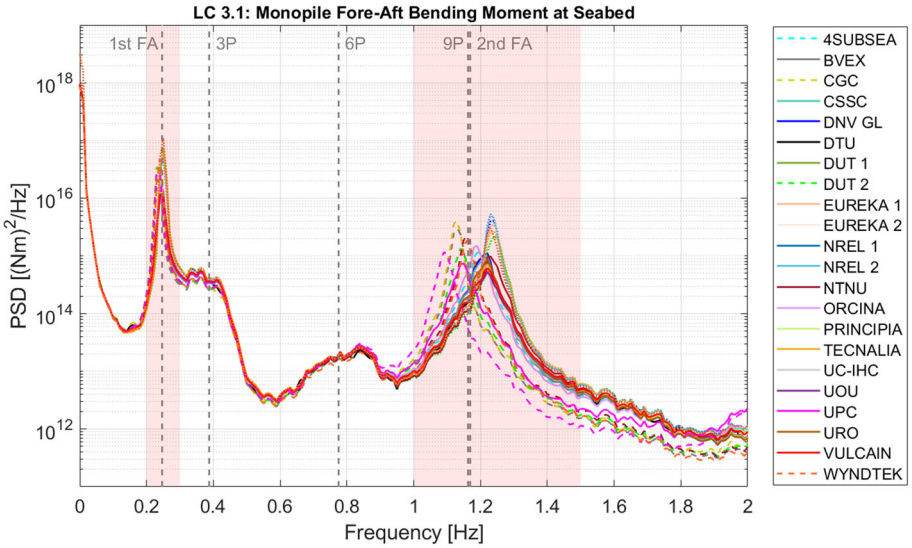

FIGURE 10 Power spectral density (PSD) of the monopile fore–aft bending moment at the seabed in load case (LC) 3.1

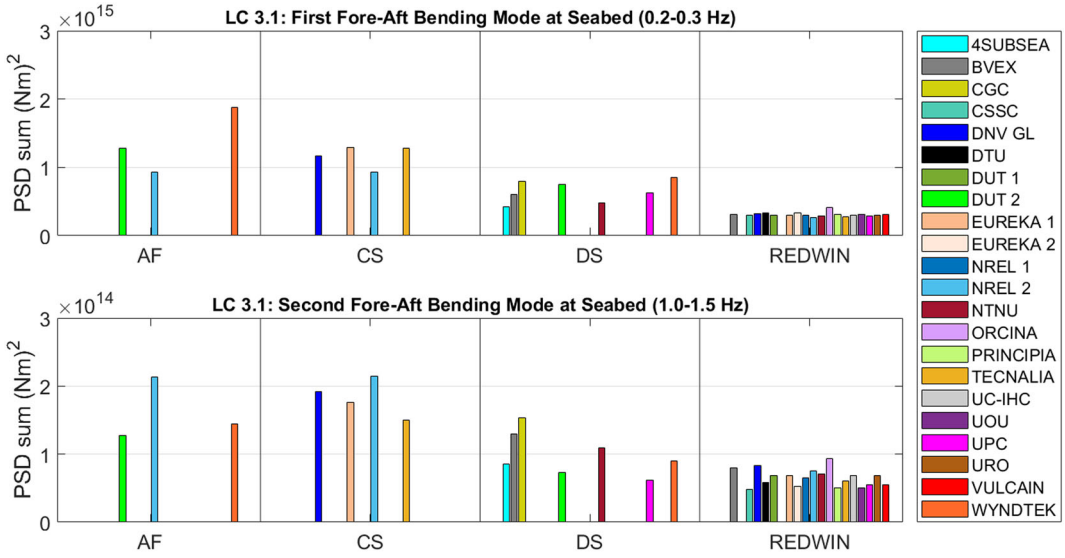

FIGURE 11 Power spectral density (PSD) sums of the fore–aft bending moment at the seabed in load case (LC) 3.1

6.4 | Wave-only simulations results: Load Case 4.2

Load Case 4.2 analyzes the response of the system under irregular waves. Load Case 4.2 is a wave-only load case. With a focus on the SSI model, a simple modeling approach was used for the hydrodynamic forces. Table 4 provides the settings that were used for the load cases that involve marine conditions to try to replicate the same input loading across participants and simulation tools.

TABLE 4 Prescribed settings for marine conditions

Hydrodynamic forces	Wave kinematics	Seawater density
Relative form of Morison equation (without corrections) Drag coefficient (C_D) = 1 Inertia coefficient (C_M) = 2	Linear (first-order) waves No wave stretching No directional spreading	1025 kg/m^3 (International Electrotechnical Commission[3])

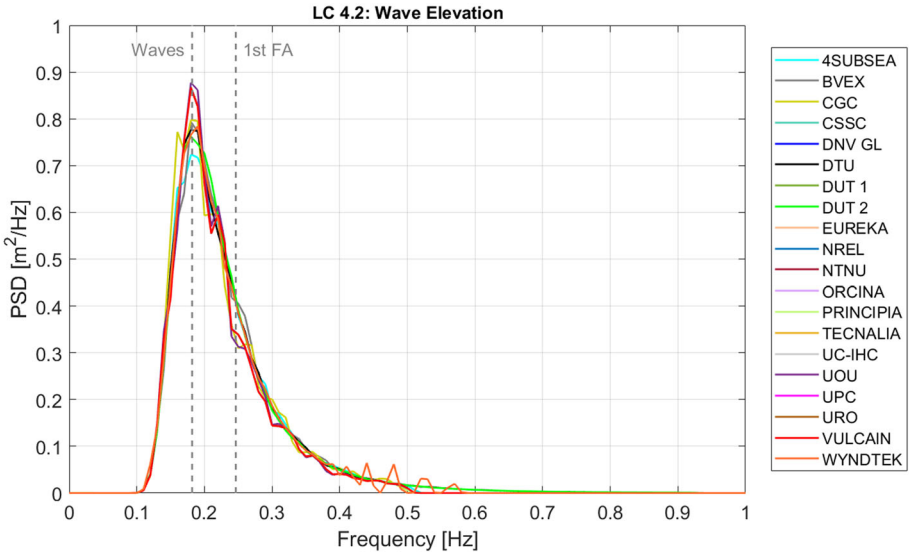

FIGURE 12 Power spectral density (PSD) of the wave elevation in load case (LC) 4.2 ($H_s = 1.25$ m, $T_p = 5.5$ s, $\gamma = 1.0$)

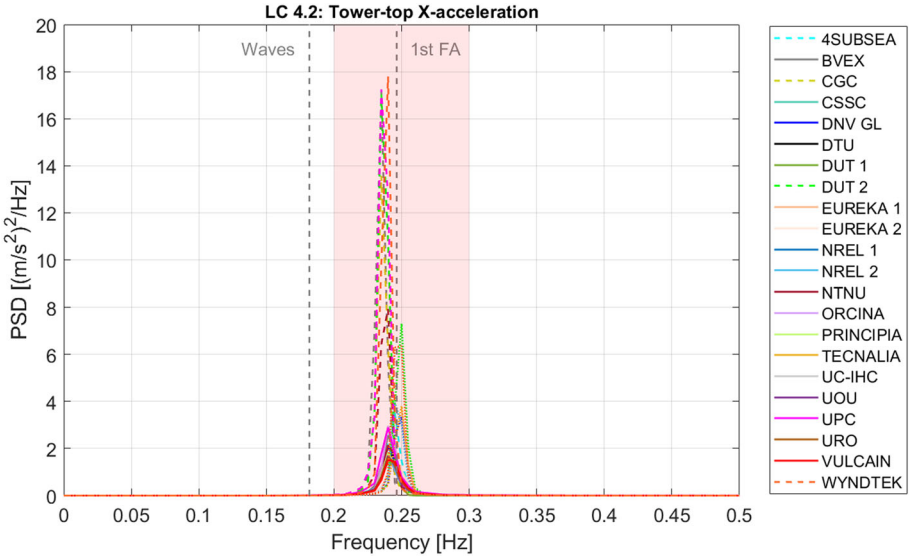

FIGURE 13 Power spectral density (PSD) of the tower-top X-acceleration in load case (LC) 4.2

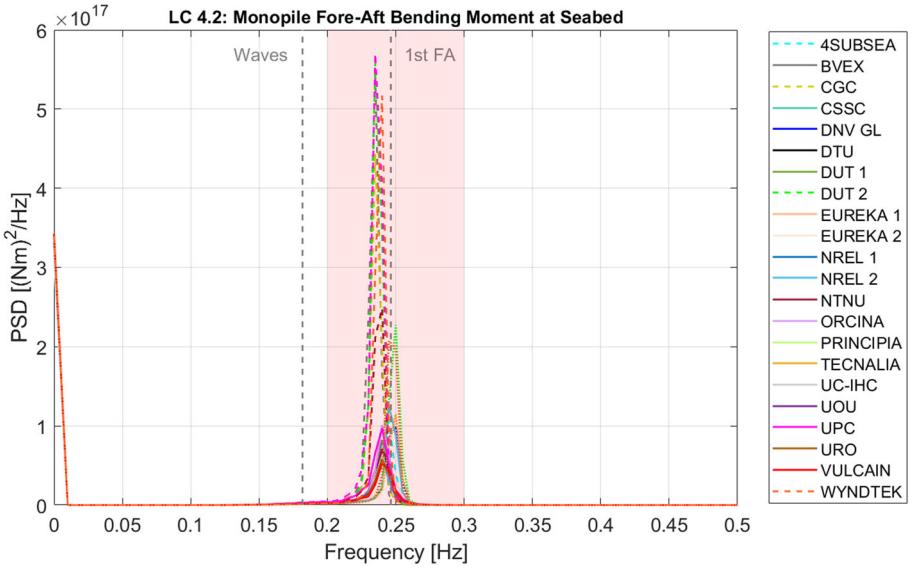

FIGURE 14 Power spectral density (PSD) of the monopile fore-aft bending moment at the seabed in load case (LC) 4.2

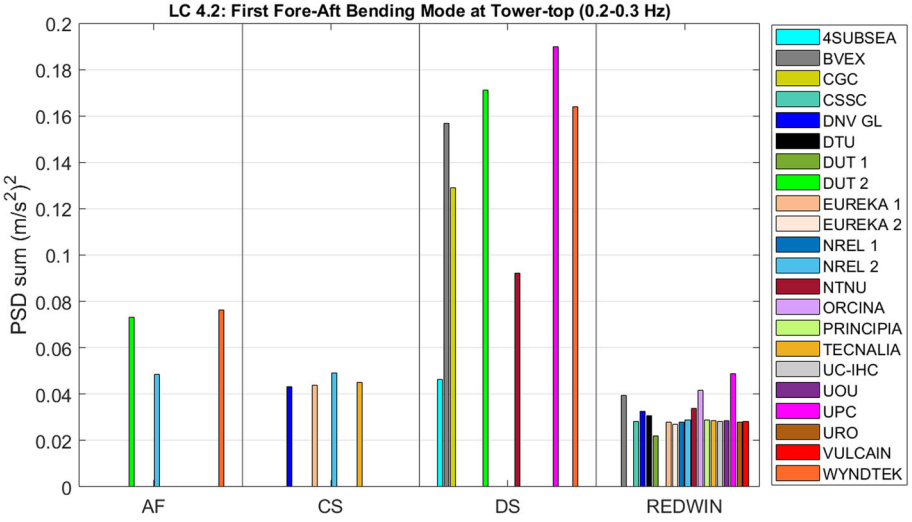

FIGURE 15 Power spectral density (PSD) sum of the tower-top X-acceleration in load case (LC) 4.2

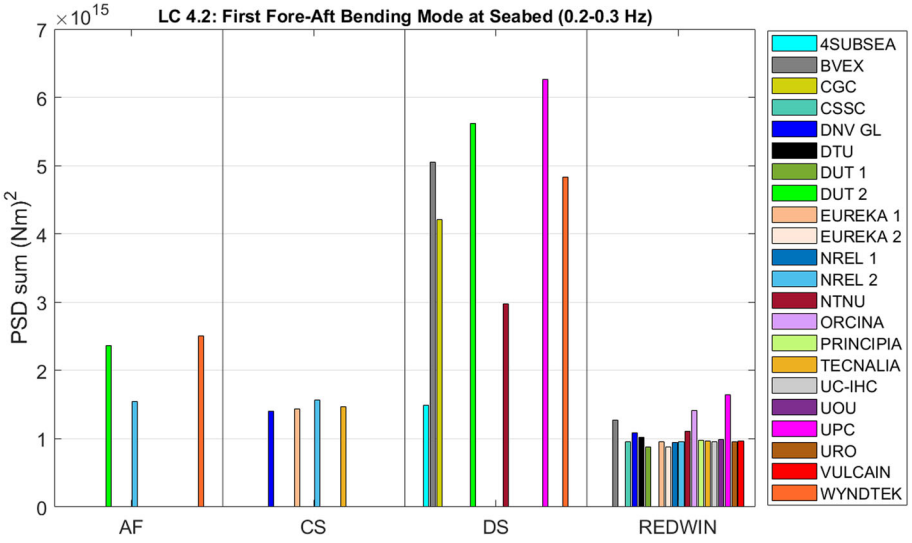

FIGURE 16 Power spectral density (PSD) sums of the fore–aft bending moment at the seabed in load case (LC) 4.2

Figure 12 shows the wave elevation spectrum in Load Case 4.2. The peak-spectral wave frequency ($1/T_p$) and the first fore–aft bending mode are also included in the figure with vertical dashed lines. The frequency range between 0.1 and 0.5 Hz contains most of the energy in the wave spectrum. This wave-only condition can only excite the first bending mode of the structure.

Figures 13 and 14 show the PSD of the tower-top acceleration along the *x*-axis and the monopile fore–aft bending moment at the seabed. Figures 15 and 16 show the associated PSD sums for the frequency range between 0.2 and 0.3 Hz, representative of the first fore–aft bending mode response. The line styles, output locations, and postprocessing in terms of PSD sums are the same as the one presented for the wind-only conditions. In this case, the largest response occurs for the DS approach, and it is likely due to the slightly lower frequency compared to the other solutions. This lower frequency locates the structural mode in a region where the wave energy is higher. As already observed in the wind-only condition, 4Subsea also uses the DS approach, but the response is more aligned with the REDWIN solution. For this participant, the first bending mode is slightly higher in terms of frequency than the other DS solutions (observed in Figure 13) and the SSI accounts for damping.

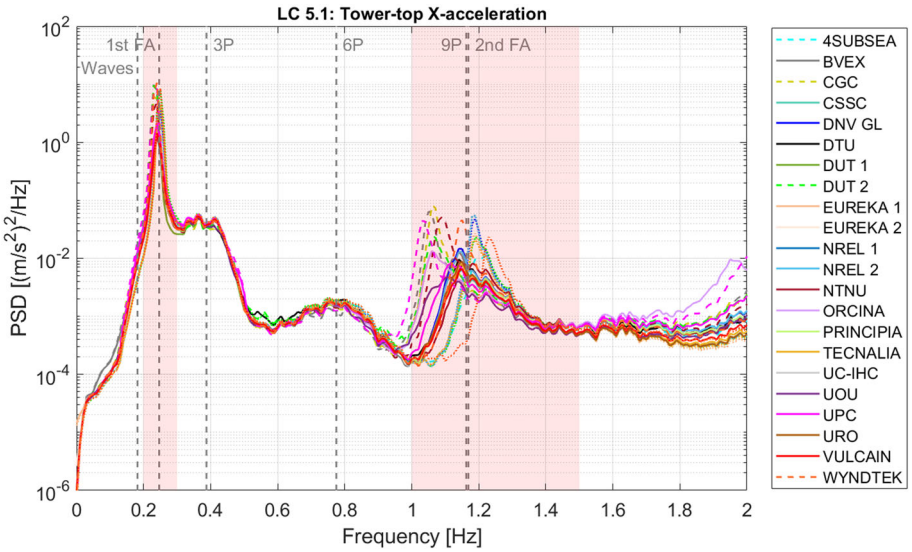

FIGURE 17 Power spectral density (PSD) of the tower-top X-acceleration in load case (LC) 5.1

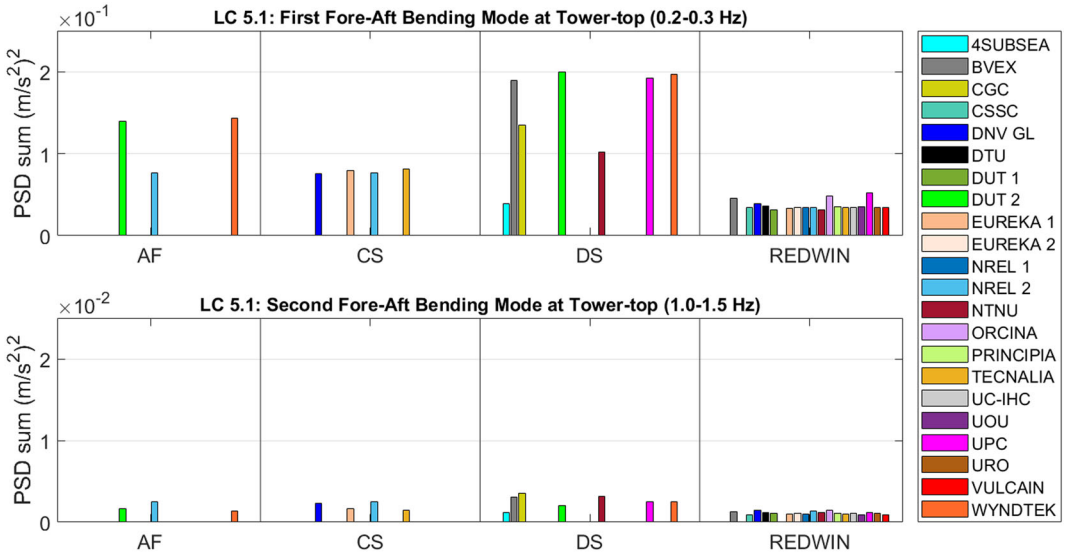

FIGURE 18 Power spectral density (PSD) sums of the tower-top X-acceleration in load case (LC) 5.1

6.5 | Combined Wind and Waves: Load Case 5.1

Load Case 5.1 combines the wind conditions studied and presented in Load Case 3.1 with the Pierson–Moskowitz wave spectrum analyzed in Load Case 4.2. Figure 17 shows the PSD of the tower-top acceleration along the *x*-axis and Figure 18 the corresponding PSD sums. Figure 17 can be compared to the one from the wind-only condition (Figure 8). As it shows, the two main differences between the wind-only and the wind/wave conditions are the response amplitude for the first fore–aft bending mode and the slight frequency shift for the second fore–aft bending mode. The amplitude of the first fore–aft bending mode is higher due to the wave excitation. The drop in frequency for the second fore–aft bending mode is due to the added mass term from the water. The PSD sums for this load case are mainly the result of the superposition of the PSD sums from the wind-only and wave-only conditions.

Figure 19 shows the monopile fore–aft bending moment at the seabed and Figure 20 the associated PSD sums. Similar to the wind-only and wave-only conditions, the response of the REDWIN approach is the smallest for the first and second fore–aft bending modes. Also, the response of the DS with damping (4Subsea) is quite similar to the one from the REDWIN approach.

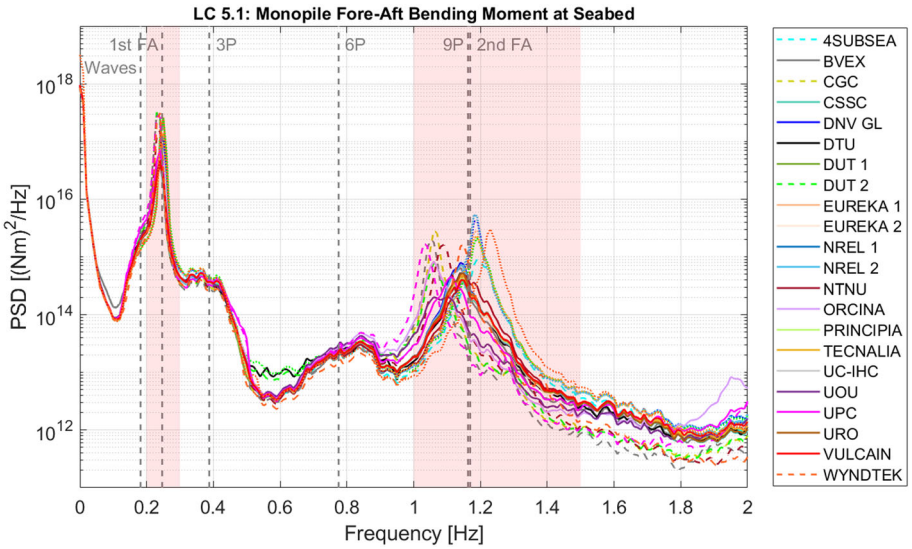

FIGURE 19 Power spectral density (PSD) of the monopile fore–aft bending moment at the seabed in load case (LC) 5.1

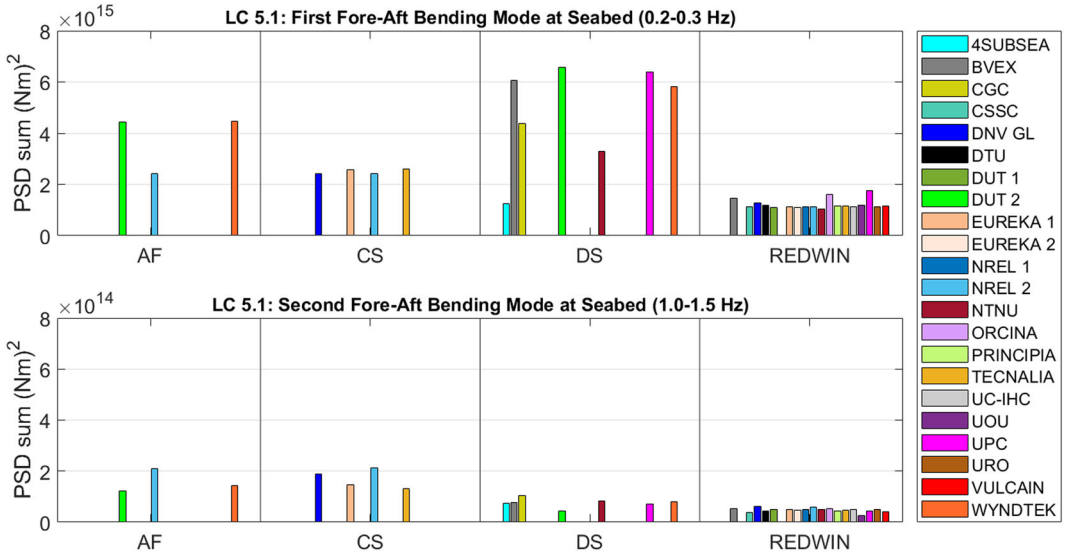

FIGURE 20 Power spectral density (PSD) sums of the fore–aft bending moment at the seabed in load case (LC) 5.1

7 | CONCLUSIONS

During the OC6 Phase II project, the REDWIN modeling capability was coupled to a variety of offshore wind modeling tools. The new capability was verified across different tools and against industry standard methods for an example monopile offshore wind system (DTU 10-MW wind turbine). Two linear (AF and CS) and two nonlinear (DS and REDWIN) SSI approaches were used during this code-to-code verification.

The REDWIN macroelement approach differs from traditional methods in the inclusion of plasticity and hysteretic damping. It requires more elaborate inputs (e.g., stiffness matrix and load–displacement curves at the seabed) to characterize the SSI. However, it models the hysteretic damping internally. This is a great advantage because the energy dissipated by the SSI is not easy to quantify and include in a numerical model. On the one hand, traditional methods have often employed a viscous damping matrix at the seabed or dashpot elements along the monopile with viscous damping. In these cases, the damping forces are proportional to the velocity. On the other hand, the hysteretic damping included in the REDWIN macroelement is dependent on the displacement trajectories. This hysteretic damping is inherently nonlinear: Larger displacement loops result in more energy dissipated. The differences between these two damping approaches would be especially noticeable at high frequency ranges, where the displacements are relatively small, but the velocities are high. The proper characterization of this soil damping is especially important in idling and wind–wave misalignment conditions.

The support structure loads at the first and second bending mode are the smallest when using the REDWIN macroelement compared to the other modeling approaches, for all load cases analyzed. This would mean a lower fatigue estimate using the REDWIN model. Although no validation was done here to assess the accuracy of the REDWIN capability, this validation was achieved within the REDWIN project and the lower fatigue estimate would mean that OWT designs could remove some conservancy. The differences observed in the loads between the REDWIN and the traditional methods are mainly due to small differences in terms of system eigenfrequencies because of the foundation flexibility and the lack of damping defined in the traditional approaches.

Across the different tools that have integrated in the REDWIN modeling approach, very similar results were seen for all load cases. This verifies the accurate implementation of the REDWIN capability in these tools, making them ready for use in the design of future OWT systems.

ACKNOWLEDGEMENTS

The authors would like to thank the Norwegian Geotechnical Institute for their work in the REDWIN project to develop the capability being incorporated in OC6 Phase II and to provide the data to model the foundation as well as for their ongoing support. We would also like to thank the Norwegian University of Science and Technology for their support in developing the model for this project.

This work was authored in part by the National Renewable Energy Laboratory, operated by Alliance for Sustainable Energy, LLC, for the US Department of Energy (DOE) under Contract No. DE-AC36-08GO28308. Funding is provided by the US Department of Energy Office of Energy Efficiency and Renewable Energy Wind Energy Technologies Office. The views expressed in the article do not necessarily represent the views of the DOE or the US Government. The US Government retains, and the publisher, by accepting the article for publication, acknowledges that the US Government retains a nonexclusive, paid-up, irrevocable, worldwide license to publish or reproduce the published form of this work or allow others to do so, for US Government purposes.

PEER REVIEW

The peer review history for this article is available at https://publons.com/publon/10.1002/we.2698.

DATA AVAILABILITY STATEMENT

The modeling information and simulation results from this project will be made available to the public by the end of 2021 through the US Department of Energy Data Archive and Portal, https://a2e.energy.gov/projects/oc6.

ORCID

Roger Bergua https://orcid.org/0000-0003-4703-4729
Amy Robertson https://orcid.org/0000-0001-7448-4632
Jason Jonkman https://orcid.org/0000-0003-2990-7362
Erin Bachynski-Polić https://orcid.org/0000-0002-1471-8254
Ander Aristondo https://orcid.org/0000-0002-0802-925X

REFERENCES

1. NGI. REDWIN (Reducing cost of offshore wind by integrated structural and geotechnical design). 3D Foundation Model Library. Accessed March 23, 2020. https://www.ngi.no/eng/Projects/REDWIN-reduce-wind-energy-cost/#Reports-and-publications
2. Velarde J, Bachynski EE. Design and fatigue analysis of monopile foundations to support the DTU 10 MW offshore wind turbine. *Energy Procedia*. 2017;137:3-13. https://doi.org/10.1016/j.egypro.2017.10.330

3. International Electrotechnical Commission (IEC). Wind energy generation systems—Part 3-1: Design requirements for offshore wind turbines. Geneva, Switzerland; 2019.
4. Det Norske Veritas (DNV). *DNV-OS-J101—Design of Offshore Wind Turbine Structures*. Det Norske Veritas; 2014. https://rules.dnv.com/docs/pdf/dnvpm/codes/docs/2014-05/Os-J101.pdf
5. American Petroleum Institute (API). *RP 2A-WSD—Recommended Practice for Planning, Designing and Constructing Fixed Offshore Platforms*. American Petroleum Institute; 2014.
6. Page AM, Grimstad G, Eiksund GR, Jostad HP. A macro-element model for multidirectional cyclic lateral loading of monopiles in clay. *Comput Geotech*. 2019;106:314-326. https://doi.org/10.1016/j.compgeo.2018.11.007
7. Page AM, Grimstad G, Eiksund GR, Jostad HP. A macro-element pile foundation model for integrated analyses of monopile-based offshore wind turbines. *Ocean Eng*. 2018;167:23-35. https://doi.org/10.1016/j.oceaneng.2018.08.019
8. Page AM, Næss V, De Vaal JB, Eiksund GR, Nygaard TA. Impact of foundation modelling in offshore wind turbines: Comparison between simulations and field data. *Mar Struct*. 2019;64:379-400. https://doi.org/10.1016/j.marstruc.2018.11.010
9. Byrne BW, McAdam R, Burd HJ, et al. New design methods for large diameter piles under lateral loading for offshore wind applications. In: *Frontiers in Offshore Geotechnics III*. CRC Press; 2015:705-710. https://doi.org/10.1201/b18442-96
10. Malekjafarian A, Jalilvand S, Doherty P, Igoe D. Foundation damping for monopile supported offshore wind turbines: A review. *Mar Struct*. 2021;77:102937. https://doi.org/10.1016/j.marstruc.2021.102937
11. Katsikogiannis G, Bachynski EE, Page AM. Fatigue sensitivity to foundation modelling in different operational states for the DTU 10MW monopile-based offshore wind turbine. *J Phys Conf Ser*. 2019;1356(1):012019. https://doi.org/10.1088/1742-6596/1356/1/012019
12. Bergua R, Robertson A, Jonkman J, Platt A. *Specification Document for Offshore Code Comparison Collaboration, Continued, with Correlation and unCertainty (OC6) Phase II: Verification of an Advanced Soil-Structure Interaction Model for Offshore Wind Turbines (NREL/TP-5000-79938)*. National Renewable Energy Laboratory (NREL). 2021. https://www.nrel.gov/docs/fy21osti/79938.pdf
13. Bortolotti P, Canet Tarres H, Dykes KL, Merz K, Sethuraman L, Verelst D, Zahle F. IEA Wind TCP Task 37: Systems Engineering in Wind Energy-WP2.1 Reference Wind Turbines. 2019. https://www.nrel.gov/docs/fy19osti/73492.pdf
14. Anaya-Lara O, Tande JO, Uhlen K, Merz K. Appendix. In: Anaya-Lara O, Tande JO, Uhlen K, Merz K, eds. *Offshore Wind Energy Technology*. John Wiley & Sons; 2020. https://doi.org/10.1002/9781119097808.app
15. Damiani R, Jonkman J, Hayman G. *SubDyn User's Guide and Theory Manual (NREL/TP-5000-63062)*. National Renewable Energy Laboratory (NREL). 2015. https://www.nrel.gov/wind/nwtc/assets/downloads/SubDyn/SubDyn_Manual.pdf
16. Jonkman J, Musial W. *Offshore Code Comparison Collaboration (OC3) for IEA Wind Task 23 Offshore Wind Technology and Deployment (NREL/TP-5000-48191)*. National Renewable Energy Laboratory (NREL). 2010. https://www.nrel.gov/docs/fy11osti/48191.pdf
17. Popko W, Vorpahl F, Zuga A, et al. Offshore Code Comparison Collaboration Continuation (OC4), Phase I—Results of Coupled Simulations of an Offshore Wind Turbine with Jacket Support Structure (NREL/CP-5000-54124). National Renewable Energy Laboratory (NREL). 2012. https://www.nrel.gov/docs/fy12osti/54124.pdf
18. Robertson A, Jonkman J, Musial W, Vorpahl F, Popko W. Offshore code comparison collaboration, continuation: Phase II results of a floating semisubmersible wind system (NREL/CP-5000-60600). National Renewable Energy Laboratory (NREL). 2013. https://www.nrel.gov/docs/fy14osti/60600.pdf
19. Robertson AN, Wendt FF, Jonkman JM, et al. OC5 Project Phase I: Validation of hydrodynamic loading on a fixed cylinder (NREL/CP-5000-63567). National Renewable Energy Laboratory (NREL) 2015. https://www.nrel.gov/docs/fy15osti/63567.pdf
20. Robertson AN, Wendt F, Jonkman JM, et al. OC5 Project Phase Ib: validation of hydrodynamic loading on a fixed, flexible cylinder for offshore wind applications (NREL/JA-5000-66648). National Renewable Energy Laboratory (NREL). 2016. https://doi.org/10.1016/j.egypro.2016.09.201
21. Robertson AN, Wendt F, Jonkman JM, et al. OC5 project phase II: validation of global loads of the DeepCwind floating semisubmersible wind turbine. *Energy Procedia*. 2017;137:38-57. https://doi.org/10.1016/j.egypro.2017.10.333
22. Robertson AN, Jonkman J, Wendt FF, et al. Verification of a Numerical Model of the Offshore Wind Turbine From the Alpha Ventus Wind Farm Within OC5 Phase III (NREL/CP-5000-70878). National Renewable Energy Laboratory (NREL). 2018. https://doi.org/10.1115/OMAE2018-77589
23. Popko W, Robertson A, Jonkman J, et al. Validation of numerical models of the offshore wind turbine from the alpha ventus wind farm against full-scale measurements within OC5 Phase III. In: *ASME 2019 38th International Conference on Ocean, Offshore and Arctic Engineering*. American Society of Mechanical Engineers Digital Collection. 2019. https://doi.org/10.1115/OMAE2019-95429

How to cite this article: Bergua R, Robertson A, Jonkman J, et al. OC6 Phase II: Integration and verification of a new soil–structure interaction model for offshore wind design. *Wind Energy*. 2021;1-18. doi:10.1002/we.2698